GROWTH RATE OF CdS BY VAPOR TRANSPORT IN A CLOSED AMPOULE

Ching-Hua Su
Universities Space Research Association
Space Science Laboratory
NASA Marshall Space Flight Center
Huntsville, AL 35812 USA

Abstract

Vapor transport of CdS in a closed ampoule due to a temperature gradient was investigated. Comparisons between the theoretical and experimental growth rate for the following conditions were discussed: (1) with and without the presence of Ar vapor, (2) convective contribution to the growth rate in the vertical stabilized and horizontal configurations, and (3) the effect of starting material composition on the growth rate. It was found that Cd reacts with fused silica ampoule and causes the contamination of CdS sample.

1. INTRODUCTION

Crystal growth by vapor transport has been investigated for many years because it allows the high melting compound semiconductors to be grown at a lower temperature. The diffusive and convective vapor transport in a closed system of GeSe-GeI_4 has been analyzed by Wiedemeier et al. [1-2]. In this paper, the transport rate of CdS in a closed ampoule has been analyzed for the vertical stabilized and horizontal configurations. The effect of the presence of an inert gas is also discussed. The theory of transport kinetics will be given in section 2. The experimental procedures will be described in section 3. Finally, comparison between the theoretical and experimental results and some discussion will be presented in section 4 and 5, respectively.

2. THEORY

The crystal growth process of transferring vapor species from source to crystal can be divided into three steps:

(1) the sublimation of species from source to the vapor phase

(2) the transport of species through the vapor phase

(3) the condensation of vapor species on the crystal surface.

We can consider crystal growth as these three processes occurring in series. Thus it is the slowest of the processes which determines the growth rate. In general, the transport of species through the vapor phase, or step (2), is much slower than the

reactions occurring at the solid-vapor interface. Therefore, throughout this paper, we will only consider the kinetics of step (2) and assume that equilibrium is always established between the solid phase and the vapor immediately adjacent to it.

The mass transfer in a multi-component gas mixture is given by the equation of flux of the general form:

$$J_i = -D_i \text{ grad } N_i + UN_i \qquad (1)$$

where J_i is the flux of species i with concentration N_i, D_i is the corresponding diffusion coefficient. The first term is the diffusive contribution to the flux. U is a flow velocity which acts on the gas as a whole, or Stefan flow, and is the result of the change in volumes or pressures during the sublimation and condensation reactions. In the presence of a gravitational field, the contribution of a convective motion should be included in the flow velocity U in the second term.

2.1 Diffusive transport without the presence of an inert gas

For a II-VI compound AB, the predominant vapor species are usually A and B_2. The vapor species of S have various forms of S_n molecule with n from 1 to 8. However, in the temperature of interest, greater than 800°C, S_2 is the predominant species [3]. We will assume that the vapor phase consists of A(g) and B_2(g) species and they behave ideally. Then for an ampoule as shown in Fig. 1, with the source surface at x = 1 and T = T(1) and the crystal surface at x = 0 and T = T(0), eq. (1) becomes:

$$J_A = - \frac{D}{RT} \frac{dP_A}{dx} + \frac{U}{RT} P_A \qquad (2)$$

$$J_{B_2} = - \frac{D}{RT} \frac{dP_{B_2}}{dx} + \frac{U}{RT} P_{B_2} \qquad (3)$$

Adding eq. (2) and (3) and noting that total pressure, $P_T = P_A + P_{B_2}$, is constant, we have

$$J_A + J_{B_2} = \frac{UP_T}{RT} . \qquad (4)$$

The growth rate of AB(s) compound is

$$J = J_A = 2J_{B_2}. \qquad (5)$$

Substituting J into eq. (4) and eliminating U in terms of J in eq. (2) and (3), we have

$$J = J_A = - \frac{D}{RT} \frac{dP_A}{dx} + \frac{3}{2} \frac{JP_A}{P_T} \qquad (6)$$

$$J = 2J_{B_2} = - \frac{2D}{RT} \frac{dP_{B_2}}{dx} + \frac{3JP_{B_2}}{P_T} . \qquad (7)$$

Assuming D is independent of the vapor composition and D and T are constant within the small temperature range of T(0) and T(1), we can integrate eqs. (6) and (7) from x = 0 to 1.

$$P_A(x) - \frac{2P_T}{3} = (P_A(1) - \frac{2P_T}{3}) \exp \left[\frac{3}{2} \frac{JRT_a}{DP_T} (x - 1)\right] \qquad (8)$$

$$P_{B_2}(x) - \frac{P_T}{3} = (P_{B_2}(1) - \frac{P_T}{3}) \exp \left[\frac{3}{2} \frac{JRT_a}{DP_T} (x - 1)\right] \qquad (9)$$

where the average temperature, T_a, is approximated by

$$T_a = \frac{T(0) + T(1)}{2} . \tag{10}$$

The transport rate, J, can be obtained from either eq. (8) or (9):

$$J = \frac{2}{3}\frac{DP_T}{RT_a l}\ln\left\{\frac{P_A(1) - \frac{2P_T}{3}}{P_A(0) - \frac{2P_T}{3}}\right\} = \frac{2}{3}\frac{DP_T}{RT_a l}\ln\left\{\frac{P_{B_2}(1) - \frac{P_T}{3}}{P_{B_2}(0) - \frac{P_T}{3}}\right\}. \tag{11}$$

The partial pressures of A and B_2, P_A and P_{B_2}, for a narrow homogeneity range compound can vary over several orders of magnitude from A-saturated to B-saturated condition. However, the Gibbs energy of formation for the gas phase is, almost independent of the deviation from stoichiometry, a function of temperature only. A least square fit to the CdS data between 629 and 789°C determined by Goldfinger et al. [4] gives:

$$\log_{10}\left(P_{Cd}^2 P_{S_2}\right) = -34492.1/T + 20.9322 \tag{12}$$

where P is in atm and T in K.

A quantity $\alpha(1)$, defined as $P_{Cd}(1)/P_{S_2}(1)$ [5], measuring the deviation of stoichiometry for the source material, is used to calculate $P_{Cd}(1)$, $P_{S_2}(1)$, $P_{Cd}(0)$, and $P_{S_2}(0)$. First, $P_{Cd}(1)$ and $P_{S_2}(1)$ can be obtained from T(1), $\alpha(1)$, and eq. (12), then $P_{Cd}(0)$ and $P_{S_2}(0)$ are calculated from T(0), eq. (12) and $P_T \equiv P_{Cd}(1) + P_{S_2}(1) = P_{Cd}(0) + P_{S_2}(0)$. Finally, the growth rate J is calculated by eq. (11) after a reasonable estimate of D.

2.2 Diffusive transport in the presence of an inert gas

The vapor species in the ampoule are A, B_2, and Z, where Z is the inert species. The flux equations for A and B_2 are similar to eqs. (2) and (3). Since there is no mass transfer for Z, the net flux of the inert gas species is zero,

$$J_Z = -\frac{D}{RT}\frac{dP_z}{dx} + \frac{U}{RT}P_Z = 0 \qquad (13)$$

Eq. (13) shows that the flux due to a constant flow velocity U from the source to the crystal is balanced by a diffusive flux resulting from a concentration gradient.

Following the same procedure as described in 2.1, we have the same equations as eq. (8), (9), and (11) for the pressure profiles and growth rate. The pressure of Z is given by

$$P_Z(x) = P_Z(1)\exp\left\{\frac{3}{2}\frac{JRT_a}{DP_T}(x-1)\right\} \qquad (14)$$

However, in these equations, eqns. (8), (9), (11), and (14), the total pressure is $P_T(x) = P_A(x) + P_{B_2}(x) + P_Z(x)$. The procedure of the numerical calculation for CdS in the presence of inert gas Z is the following.

First, the number of moles of Z, N_Z, can be calculated assuming ideal gas law for Z,

$$N_Z = \frac{P_Z'V}{RT'} = \int_0^1 \frac{P_Z(x)A}{RT}\,dx \qquad (15)$$

where P_Z' and T' are the pressure and temperature at the condition of sealed-off, V is the free volume of the ampoule, and A the cross section area of the ampoule. Assuming A is constant and T = T_a = constant, we can integrate eq. (15) with $P_Z(x)$ given by eq. (14)

$$P_Z(1) = \frac{3}{2}\frac{JRT_a}{DP_T}\frac{P_Z'\frac{V}{T'}}{\frac{A}{T_a}}\left\{1 - \exp\left[\frac{3}{2}\frac{JRT_a}{DP_T}(-1)\right]\right\}^{-1} . \qquad (16)$$

The quantity $\frac{V/T'}{A/T_a}$ can be obtained from the profiles of the temperature and volume or simply approximated as lT_a/T'. For a given $\alpha(1)$, $P_{Cd}(1)$ and $P_{S_2}(1)$ can be calculated from T(1) and eq. (12) as described in 2.1. Then an initial value is given for J which enables us to solve $P_Z(1)$ from eq. (16) by an iterative process because $P_T = P_{Cd}(1) + P_{S_2}(1) + P_Z(1)$ also appears in the equation. Then $P_{Cd}(0)$, $P_{S_2}(0)$, and $P_Z(0)$ are calculated by eqs. (8), (9), and (14) and the calculated value for $P_{Cd}^2(0)\,P_{S_2}(0)$ obtained. Finally, a trial and error routine [6] is used to vary J until the calculated value for $P_{Cd}^2(0)\,P_{S_2}(0)$ agrees within 0.01% to the experimental value given by eq. (12).

2.3 Contribution of the convective transport

In a two-dimensional enclosure shown in Fig. 2a, if there is a positive temperature gradient such as in Fig. 2b, perpendicular to the gravitational field which directs toward -y direction, then thermal convection flows in the pattern as shown in Fig. 2a. The interaction between this flow and a concentration profile of $\frac{\partial n}{\partial x} > 0$ as in Fig. 2b gives rise to a transversal

concentration gradient $\frac{\partial n}{\partial y} > 0$ as shown in Fig. 2c. The net flux resulting from this gradient is the convective contribution to the total flux and is in the order of $V_x d \frac{\partial n}{\partial y}$ ($= V_x n|_{y=0} - V_x n|_{y=l}$).

Klosse et al. [7] have calculated this thermal convective contribution to the total mass transfer in a rectangular enclosure due to a horizontal temperature gradient. The result is given in terms of a dimensionless quantity K which is defined as the ratio of the mass transfer of convection to diffusion:

$$J_t = (1 + K)\, J_D \tag{17}$$

where J_t is the total flux and J_D the diffusive flux given in 2.1 and 2.2. Their expression for K is

$$K = [A/(N_{Sc}\, N_{Gr})^2 + B]^{-1} \tag{18}$$

where A and B are geometrical parameters depending on the dimension of the enclosure. The numerical values for A and B as a function of the ratio of the dimension l/d is given in fig. 4 of Ref. [7]. N_{Sc} and N_{Gr} are the Schmidt and Grashof numbers used in the fluid dynamics and are given by:

$$N_{Sc} = \eta/\rho D \tag{19}$$

$$N_{Gr} = d^3 g \beta \rho^2 [T(1) - T(0)]/\eta^2 \tag{20}$$

where η is the viscosity, ρ the density, g the gravitational force, and β the thermal expansion coefficient. Under the assumption of ideal gas for the transport fluid, ρ and β can be approximated as:

$$\rho = \sum_i \frac{P_i M_i}{RT_a} \tag{21}$$

$$\beta \equiv -\frac{1}{\rho}\frac{\partial \rho}{\partial T} = \frac{1}{T_a} \tag{22}$$

where M_i is the molecular weight of species i.

2.4 Estimation of η and D

The transport parameters, viscosity η and diffusion coefficient D, for a low pressure gas mixture can be well estimated by kinetic theory of gas [8].

2.4.1 Viscosity η

The viscosity of a one component gas phase can be calculated by assuming a Lennard-Jones 6-12 intermolecular potential $\psi(r)$ between species

$$\psi(r) = 4\varepsilon\left[\left(\frac{\sigma}{r}\right)^{12} - \left(\frac{\sigma}{r}\right)^{6}\right]. \tag{23}$$

The two interaction parameters, ε and σ, are respectively, the potential well depth and the intermolecular distance at $\psi = 0$. The viscosity is then given by

$$\eta = 26.69 \frac{\sqrt{MT}}{\sigma^2 \Omega_v} \tag{24}$$

where η in μp , T in K, σ in Å, and

$$\Omega_v = \left(\frac{A}{T^{*B}}\right) + \frac{C}{\exp(DT^*)} + \frac{E}{\exp(FT^*)} \tag{25}$$

where $T^* = \frac{kT}{\varepsilon}$ and

$A = 1.16145$, $B = 0.14874$, $C = 0.52487$

$D = 0.77320$, $E = 2.16178$, $F = 2.43787$.

The viscosity of gas mixtures at low pressures is given by

$$\eta_m = \sum_{i=1}^{n} \frac{y_i \eta_i}{\sum_{j=1}^{n} y_j \phi_{ij}} \tag{26}$$

where

$$\phi_{ij} = \frac{[1 + (\eta_i/\eta_j)^{1/2} (M_j/M_i)^{1/4}]^2}{[8(1 + M_i/M_j)]^{1/2}} \tag{27}$$

and η_i and y_i are the viscosity of pure-component i and mole fraction of species i, respectively.

2.4.2 Diffusion coefficient D

The diffusion coefficient for a binary gas system at low pressure can be estimated by

$$D_{AB} = 1.858(10^{-3}) T^{3/2} \frac{[(M_A + M_B)/M_A M_B]^{1/2}}{P \sigma_{AB}^2 \Omega_D} \tag{28}$$

where D_{AB} is in cm^2/s, T in K, P in atm, and σ_{AB} in Å.

The simple rules for the interaction paramters, ε_{AB} and σ_{AB}, between the vapor species A and B are often employed:

$$\varepsilon_{AB} = (\varepsilon_A \varepsilon_B)^{1/2}$$
$$\sigma_{AB} = \frac{\sigma_A + \sigma_B}{2} \qquad (29)$$

where ε_A, σ_A and ε_B, σ_B are respectively, the potential parameters for pure component A and B, and Ω_D in eq. (28) is given by

$$\Omega_D = \frac{A}{T^{*B}} + \frac{C}{\exp(DT^*)} + \frac{E}{\exp(FT^*)} + \frac{G}{\exp(HT^*)} \qquad (30)$$

where $T^* = kT/\varepsilon_{AB}$, A = 1.06036, B = 0.15610, C = 0.19300, D = 0.47635, E = 1.03587, F = 1.52996, G = 1.76474, H = 3.89411.

In the presence of an inert gas, the diffusion coefficient is approximated by substituting total pressure for P in the denominator of eq. (28).

3. EXPERIMENTAL

Source materials of CdS were supplied by Eagle-Picher Inc. in the form of a mixture of small chunks and powder. The ampoules were 16 mm OD, 3 mm wall thickness silica tubes. After cleaning with distilled H_2O, HF, methanol, and acetone, the ampoules were baked out at 1140°C for 3 hrs. Then it was sealed off under 10^{-2} torr vacuum or Ar pressure after CdS was loaded.

Typically, the ampoule is 14 cm long with CdS source covering about 3 cm of its length. The ampoule was then placed inside a four-zone transparent furnace mounted in such a way that it can be tilted to give different configurations. Fig. 3 shows the typical temperature profile used for the vapor transport.

Experimental condition for CdS vapor transport can be divided into three categories:

(1) Ampoules were sealed off under vacuum. In order to compare the transport rates between vertical stabilized (hot end on the top) and horizontal configurations, all the source materials were transported using the same ampoule in the two configurations.

(2) Ampoules were sealed under different Ar pressures and transport was stopped after about 2 weeks. The ampoule was then broken and transport rate was calculated from the amount of CdS collected at the cold end.

(3) In an attempt to control the $\alpha(1)$ values of the source materials, CdS were annealed under Cd pressure before loading into the transported ampoules. First, CdS source materials about 6 gms and pure Cd about 5 gms from Cominco Ltd, American were loaded into an annealing ampoule and sealed under vacuum. With the help of 5 cm wide ceramic heat barrier, a temperature profile as shown in Fig. 4 was achieved with CdS at 880°C and Cd at 393±3°C. The ampoule was opened after 22 hrs. anneal and CdS was used as source material for the subsequent transport experiment.

4. RESULTS

4.1 Theoretical Calculation

The transport rate of CdS is calculated by the procedure described in section 2. Table 1 gives the intermolecular potential parameters used for Cd, S_2, and Ar vapor species. The values for Cd are taken from a recent determination by Su et al. [9] using optical absorption technique and those for S_2 are the results of a theoretical calculation [10]. The only experimental viscosity data available are for Ar vapor between 0 and 827°C and the calculated values agree with them to ±2.2% when the interaction parameters in Table 1 are used in eqs. (24) and (25).

4.1.1 Without the presence of an inert gas

Fig. 5 shows the growth rate for T(1) at 880°C as a function of $\Delta T \equiv T(1) - T(0)$ for various values of $\alpha(1)$. As the source material approaching congreuntly sublimation, or $\alpha(1) = 2.0$, the growth rate increases rapidly. In fact, in examining the growth rate equation, eq. (11), we see that the growth rate is infinite when $\alpha = 2.0$. This means that when $\alpha(1)$ gets within a certain range about 2.0, the vapor transport rate is so fast that the reaction at the solid-vapor interface becomes the rate-limited step. The figure also shows that growth rate reaches saturation at $\Delta T = 30$°C and a larger ΔT does not effectively increase the transport rate. Here we only show the results for several values of $\alpha(1)$ between 0.1 and 10. The actual limits of $\alpha(1)$ for CdS at 880°C can be obtained from the experimental partial pressures at the three-phase loops which are not known at present. In

principle, it can have value much higher than 10 for Cd-saturated and much lower than 0.1 for Te-saturated condition. Fig. 6 shows the partial pressure profiles for Cd and S_2 along a 10 cm ampoule for two values of ΔT, 10 and 30°C for $T(1) = 880°C$ and $\alpha(1) = 3.0$. According to eqs. (6) and (7), the transport rate resulting from Stephen flow is proportional to the partial pressure while the contribution from diffusion is proportional to the pressure gradient and the net transport rates for Cd and S_2 have to satisfy the equality $J_{Cd} = 2J_{S_2}$. As we can see from Fig. 6 the diffusive flux for Cd is actually from crystal to source for a source material of $P_{Cd}/P_{S_2} > 2.0$. Fig. 7 shows that for fixed $\alpha(1)$ and ΔT the transport rate is almost constant for $T(1)$ between 800 and 1000°C. Because as $T(1)$ increases, although partial pressures increase, the corresponding diffusion coefficient decreases. The contribution of convective transport for the horizontal configuration is also calculated as described in 2.3 and found to be negligible, $K \equiv \frac{J_t}{J_D} - 1$ is in the order of 10^{-9} or less for a 10 cm long, 1 cm diameter ampoule.

4.1.2 In the presence of Ar vapor

The effect of Ar pressure on the growth rate has been calculated and is shown in Fig. 8. The Ar pressure in the figure is the value at 25°C sealed-off condition. The actual Ar pressure inside the ampoule at 880°C is about four times higher. The growth rate at an Ar pressure of 0.05 atm decreases more than two orders of magnitude from its value at $P_{Ar} = 0$. However, the differences between J for various values

of $\alpha(1)$ become smaller when Ar vapor is introduced. The same kind of plot in a log-log scale is shown in Fig. 9 and P_{Ar} is extended to 30 atm. The transport rate for a horizontal configuration, including the convective contribution, is shown as dashed lines. This contribution is essentially negligible for P_{Ar} less than 1 atm. Although the transport rate reaches a maximum at a P_{Ar} value about 7 atm for the horizontal configuration, the value of K, ratio of convective to diffusive contribution, still increases slowly as P_{Ar} increases and is about 12 at P_{Ar} = 30 atm. The sum of the partial pressures, $P_{Cd} + P_{S_2}$, at 880°C are 1.915 (10^{-3}) and 2.401 (10^{-3}) atm for α = 2.0 and 10.0, respectively. For the P_{Ar} range shown in Fig. 9, P_T ($\equiv P_{Cd} + P_{S_2} + P_{Ar}$) is much greater than $P_{Cd} + P_{S_2}$. Using the approximation ln (1 - x) = -x when x << 1, in eq. (11), we have

$$J = -\frac{D}{RT_a l}\left[P_A(1) - P_A(0)\right] = -\frac{2D}{RT_a l}\left[P_{B_2}(1) - P_{B_2}(0)\right] \quad (31)$$

Since $D \propto P_T^{-1}$ and the difference in $P_A(1)$ and $P_A(0)$ is almost independent of P_T, the transport rate $J \propto P_T^{-1}$. As shown in Fig. 9, J vs P_{Ar} in a log-log plot is almost a straight line with a slope of -1.

The calculated Groshof number, N_{Gr}, for the case of ΔT = 50°C, is also presented as a function of P_{Ar} in Fig. 9 and is 3.68 at P_{Ar} = 0.1 atm and 3.25 (10^5) at P_{Ar} = 30 atm.

4.2 Experimental Results

As described in Experimental, vapor transport of CdS was performed under three different conditions:

(1) Ampoule CdS-1 was sealed off under vacuum and transport rate was obtained from the time required to transfer all material from hot to cold end. This was done for both vertical stabilized and horizontal configurations. It is known that vertical stabilized configuration produces a mode where gravity driven convection should be at its minimum or absent. Transport rates for both configurations were given in Table 2 and Fig. 5 and show almost no convective contribution in this case. The amount of CdS transported and the temperatures at hot and cold ends are also tabulated in Table 2.

(2) Ampoules CdS-2, 4, and 5 were sealed off under Ar pressures from 0.07 to 0.23 atm as given in Table 2. The transport rates were obtained from the amount of CdS transported in a period of about 2 weeks under horizontal configuration. They were 5-8 times slower than that of $P_{Ar} = 0$ run. Fig. 9 shows that these data agree quanitatively with the theoretical results and are in the region where convective contribution is negligible.

For the experiments in (1) and (2), nucleation started right after the temperature profile was established and occurred at many spots in the cold end of the ampoule. The largest crystal is about 0.5 x 2 x 3 mm as shown in the picture of Fig. 10.

(3) As described in Experimental, we try to control the $\alpha(1)$ values for the source materials by annealing CdS under

Cd pressure before loading into the transporting ampoules. According to Gibbs phase rule, once the temperature and P_{Cd} over the CdS source are fixed, all the thermodynamic properties of CdS are fixed. From the vapor pressure equation for Cd:

$$\log_{10} P_{Cd} = -5317/T + 5.119 \qquad (32)$$

where P is in atm and T in K, we can calculate P_{Cd} inside the ampoule and the α value for the source materials can be obtained from eq. (12). In this case, CdS at 880°C and Cd at 393°C, $\alpha(1)$ is 2.45. Ampoule CdS-6 was loaded with this annealed source material and sealed under vacuum. However, there was some black residue left at the hot end after transport completed. Using energy dispersive x-ray (EDX) spectrometer, we identified the black residue to be essentially Si (or Si oxide since the atomic weight of oxygen is too low for our machine to be detected) as shown in Fig. 11. The annealing process was repeated and care was taken to minimize the possibility of contamination. Ampoules CdS-7 and 8 were loaded and sealed under vacuum. After transport completed, appreciable amount of Si were found at the hot end for both runs. The starting CdS and the CdS after anneal were examined by EDX. As shown in Fig. 12, there is no Si in the starting CdS, but a Si peak appears after the CdS was annealed. The Cd used in the anneal process was also a possible source of contamination. Therefore, the transporting set-up was used to transport pure Cd from the hot end to the cold end. Since the vapor pressure of Si is very low, this process is virtually a

distillation. However, some black Si residue was found after the second distillation. Actually, small particles of silica detached from the ampoule wall could be seen in the hot end. Therefore, the following conclusions were reached: (1) Cd attacks the silica ampoule (2) detached Si (or SiO_2) can transport inside the ampoule by some unknown mechanisms.

The annealing ampoule was graphitized by pyrolysis of methane at 1050°C for 80 minutes. CdS-9 was loaded with CdS annealed in the graphitized ampoule and transport was performed. The black residue, although in much less amount than ampoules CdS-6, 7, and 8, was found at the hot end after transport completed.

5. DISCUSSION

From the theoretical calculation, the value of $\alpha(1)$ can affect the growth rate tremendously as shown in Fig. 5. The assumption of $\alpha(1) = 2.0$ in the analyses of Bulakh [12] and Paorici et al. [13] is not justified. Ballentyne et al. [14] heated the CdS source material at about 900°C in a slow flow of Ar for 4-5 hrs. to make the material "more stoichiometric". This is also doubtful because it is not known whether the congruently sublimation composition exists inside the homogeneity range until the three phase curves of the individual partial pressure are determined. Various experiments, such as the growth rate as a function of l, $\alpha(1)$, and P_{Ar}, need different ampoules loaded with CdS of known $\alpha(1)$. The annealing method used here should fulfill

this purpose if not for the contamination of Si during anneal. The contamination of CdTe by Al and Si from quartz tube and Cd metal used as the reservoir during the annealing of CdTe was reported by Taguchi et al. [15]. Using secondary ion mass spectrometry (SIMS), Morimoto et al. [16] also found impurities of Si and Al in the remainder of the CdS source material after part of it was transported. Russell et al. [17] associated the incidence of voids in vapor grown CdS crystals with the minute particles of SiO_2 that originate from the walls of the ampoule. Recently, Su et al. [18] recognized that the reaction between Cd and silica ampoule causes the adhesion of sample to the silica wall, or "wetting", during the homogenization of HgCdTe and consequently eliminated the "wetting" problem by adopting a slower heating rate.

The comparison between the theoretical results and the transport rate of CdS-1 as given in Fig. 5 does not necessarily indicate the $\alpha(1)$ value for the CdS-1 source material to be about 10. or 0.1. In this run we transported all the source CdS and the $\alpha(1)$ value changes during the transport. The final part of the source CdS can be very Cd-rich or S-rich and needs a long time to transport.

Acknowledgments

Thanks are due to Dr. S. L. Lehoczky for the reading of the manuscript, Alice Dorries for the EDX measurement, and Jimmy Lee for the graphitization of the ampoule.

References

[1] H. Wiedemeier, D. Chandra, and F. C. Klaessig, J. Crystal Growth, 51 (1980), 345.

[2] D. Chandra and H. Wiedemeier, J. Crystal Growth, 57 (1982), 159.

[3] B. Meyer, Chem. Rev. 76 (1976), 367.

[4] P. Goldfinger and M. Jeunehomme, Trans. Farad. Soc., 59 (1963), 2851.

[5] M. M. Faktor and I. Garrett, Growth of Crystals from the Vapour (Chapman and Hall, London, 1974).

[6] J. A. Nelder and R. Mead, Computer J., 7 (1965), 308.

[7] K. Klosse and P. Ullersma, J. Crystal Growth, 18 (1973), 167.

[8] R. C. Reid, J. M. Prausnitz, and T. K. Sherwood, The Properties of Gases and Liquids (McGraw-Hill, New York, 1977).

[9] C.-H. Su, P.-K. Liao, Y. Huang, S.-S. Liou, and R. F. Brebrick, J. Chem. Phys., 81 (1984), 11.

[10] D. M. Shteingradt and V. E. Lyusternik, Russ. J. Phys. Chem., 56 (1982), 1379.

[11] R. A. Svehla, NASA Tech. Rep. R-132, Lewis Research Center, Cleveland, Ohio, 1962.

[12] B. M. Bulakh, J. Crystal Growth, 5 (1969), 243.

[13] C. Paorici and C. Pelosi, J. Crystal Growth, 35 (1976), 65.

[14] D. W. G. Ballentyne, S. Wetwatana, and E. A. D. White, J. Crystal Growth, 7 (1970), 79.

[15] T. Taguchi, J. Shirafuji, and Y. Inuishi, Jap. J. Applied Phys., 17 (1978), 1331.

[16] J. Morimoto, T. Ito, T. Yoshioka, and T. Miyakawa, J. Crystal Growth, 57 (1982), 362.

[17] G. J. Russell, N. F. Thompson, and J. Woods, J. Crystal Growth, 71 (1985), 621.

[18] C.-H. Su, S. L. Lehoczky, and F. R. Szofran, submitted to J. Applied Phys.

TABLE 1. Intermolecular Potential Parameters Used in the Calculation for Cd, S_2, and Ar Vapor Species.

Species	σ(Å)	ε(meV)
Cd	4.10	48
S_2	3.97	102*
Ar†	3.54	8

*Ref. [10] gave the parameter, Z, in Sutherland equation for viscosity. Comparing it with eq. (24), we have $1 + Z/T = \Omega_v$. ε = 102 meV gives values of Ω_v agree with $1 + Z/T$ to ±1.5% between 1000 and 1200 K.

†Ref. [11]

TABLE 2. Experimental Conditions for CdS Vapor Transport
Column 3 Indicates Whether the Source Materials Have Been Annealed Under P_{Cd} Pressure; Column 4 Gives the Ar Pressure at Room Temperature.
All runs are in horizontal configuration except the first one.

Run	Amount of Source (gm)	Annealed in P_{Cd}	P_{Ar}(atm)	T(1) in °C	T(0) in °C	Amount Transported (gm)	Time (hrs.)	Rate (mole/cms^2)
CdS-1†	1.798	No	0	880	845	1.798	59	7.5 (10^{-8})
CdS-1	1.798	No	0	880	845	1.798	52	8.5 (10^{-8})
CdS-2	1.791	No	0.23	880	835	0.13	328	9.3 (10^{-10})
CdS-4	1.803	No	0.07	895	850	0.22	306	1.8 (10^{-9})
CdS-5	1.145	No	0.13	895	850	0.19	306	1.5 (10^{-9})
CdS-6	1.239	Yes	0	880	850			
CdS-7	0.443	Yes	0	880	850	black residue left at the		
CdS-8	0.653	Yes	0	880	850	hot end, contaminated by Si		
CdS-9	0.639	Yes*	0	880	850			

†vertical stabilized configuration

*graphitized annealing ampoule

Figure Captions

Fig. 1 Schematic of transporting ampoule and temperature profile.

Fig. 2 Origin of convective mass transport (a) flow pattern of thermal convection if there is a horizontal temperature gradient as given by (b) and a gravitational field directs toward -y (b) the horizontal concentration or temperature gradient (c) the vertical concentration gradient results from the thermal convection and the concentration gradient in (b).

Fig. 3 Temperature profile of the transport experiment.

Fig. 4 Temperature profile of the annealing experiment.

Fig. 5 Transport rate J, in log scale, as a function of $\Delta T \equiv T(1) - T(0)$ at $T(1) = 880°C$, and $l = 10$ cm for various values of $\alpha(1)$.

Fig. 6 Partial pressure profiles in a 10 cm long ampoule for $T(1) = 880°C$, $\alpha(1) = 3.0$. Solid curves are for $\Delta T = 30°C$ and dashed curves for $\Delta T = 10°C$.

Fig. 7 Transport rate in log scale as a function of T(1) for $\Delta T = 30°C$, $l = 10$ cm and various values of $\alpha(1)$.

Fig. 8 Transport rate J, in log scale, as a function of Ar pressure under sealed-off condition for $T(1) = 880°C$, $l = 10$ cm, $\Delta T = 50°C$, and $\alpha(1) = 3.0$ and 10. x's mark the rate at $P_{Ar} = 0$.

Fig. 9 Transport rate plotted against Ar pressure in a log-log scale for $T(1) = 880°C$, $\alpha(1) = 3.0$, $l = 10$ cm, diameter

= 1 cm, and ΔT = 30, 50°C. Solid curves are the calculated results for the vertical stabilized configuration and dashed curves are for the horizontal configuration. Symbols are the experimental results of transport rate. Also shown is the calculated Grashof number (right scale), N_{Gr}, as a function of Ar pressure for the case of ΔT = 50°C.

Fig. 10 Picture of CdS crystals.

Fig. 11 EDX (energy dispersive x-ray) spectrum of the black residue left at the hot end after transport was completed.

Fig. 12 EDX spectra of the starting CdS and CdS after anneal. Solid curve is the spectrum of starting CdS and circles represent the curve for the CdS after annealing under Cd pressure.

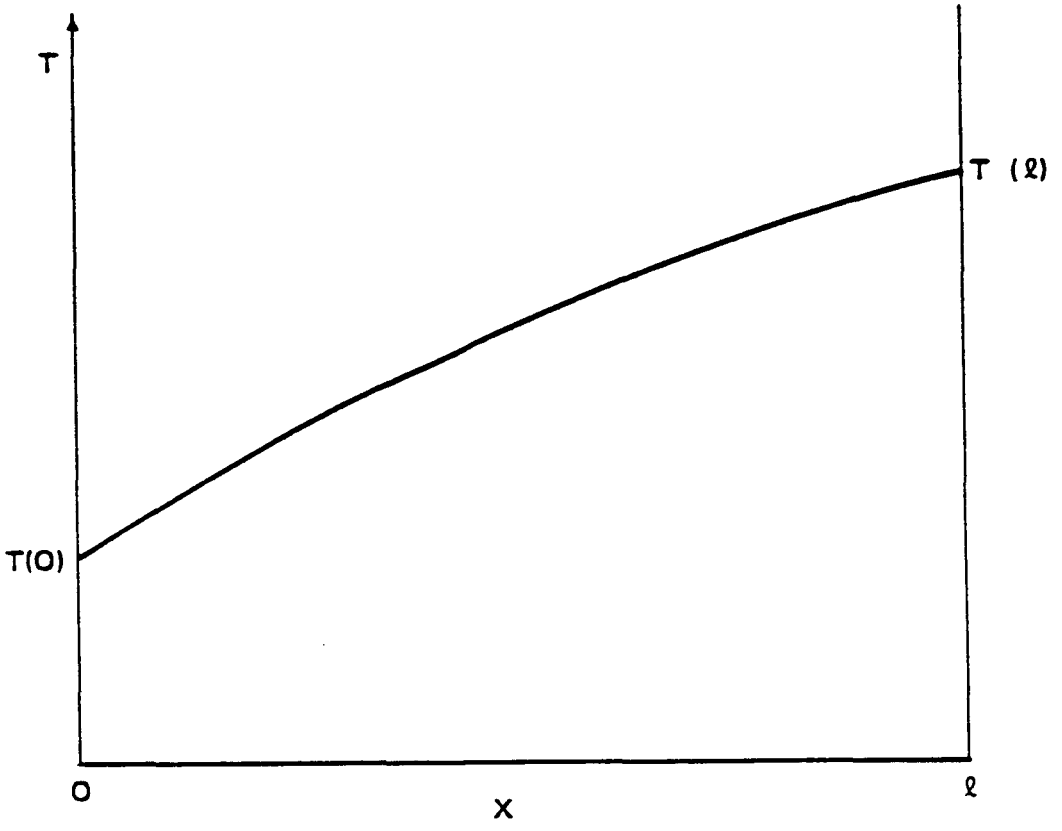
T
T (ℓ)
T(O)
O
X
ℓ

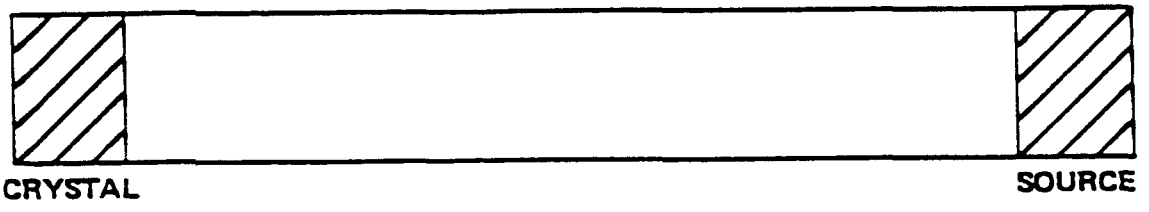
CRYSTAL
SOURCE

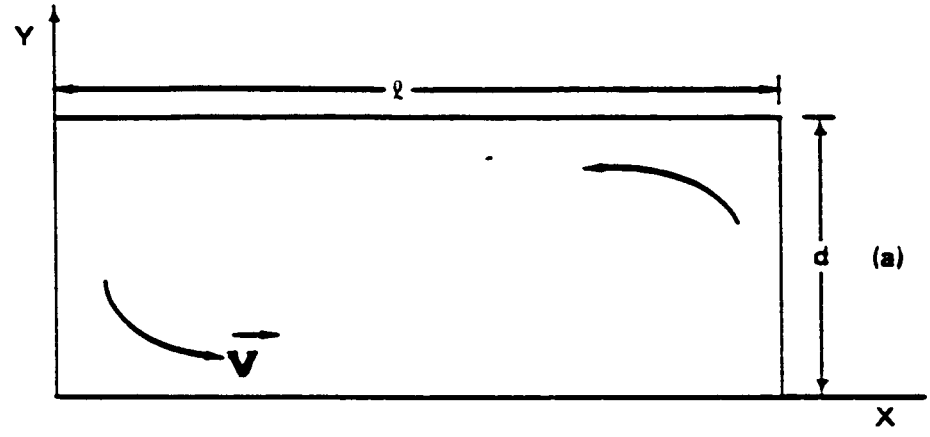
Y
ℓ
d
(a)
V
X

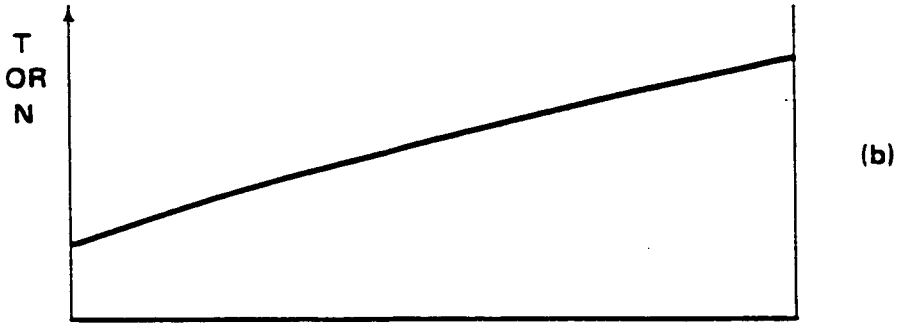
T
OR
N
(b)

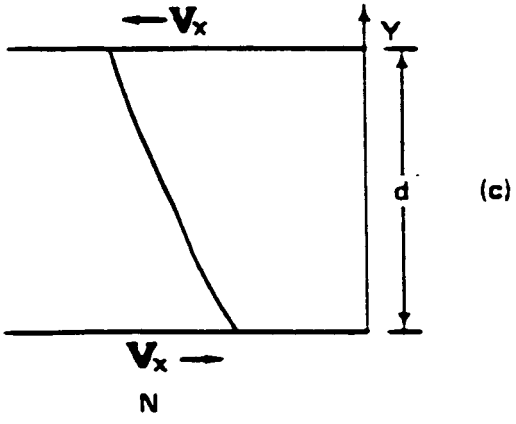
Vx
Y
d
(c)
Vx
N

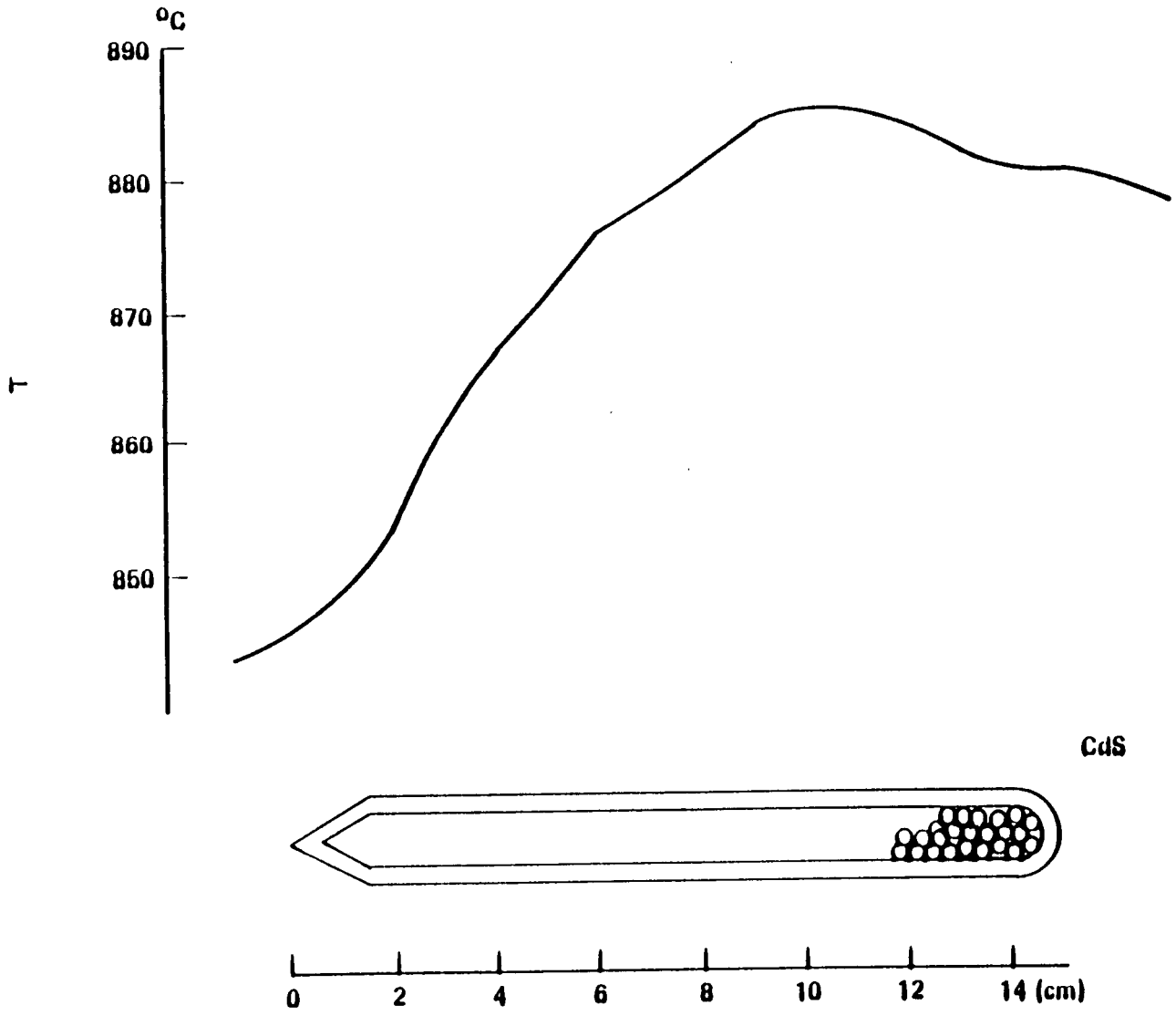
°C
890
880
870
860
850
T
CdS
0
2
4
6
8
10
12
14 (cm)

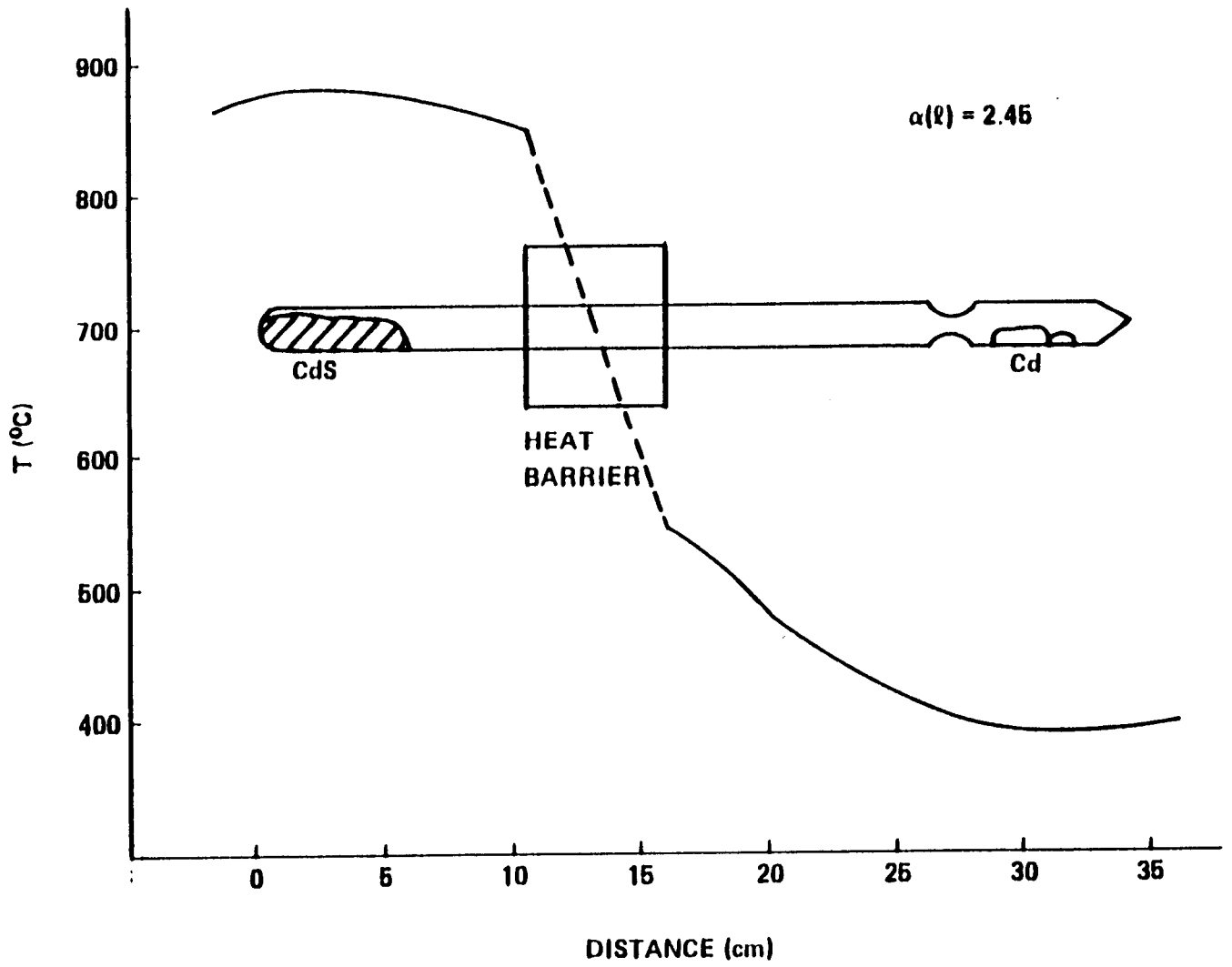
900
800
700
600
500
400
T (°C)
α(ℓ) = 2.46
CdS
Cd
HEAT
BARRIER
0
5
10
15
20
25
30
35
DISTANCE (cm)

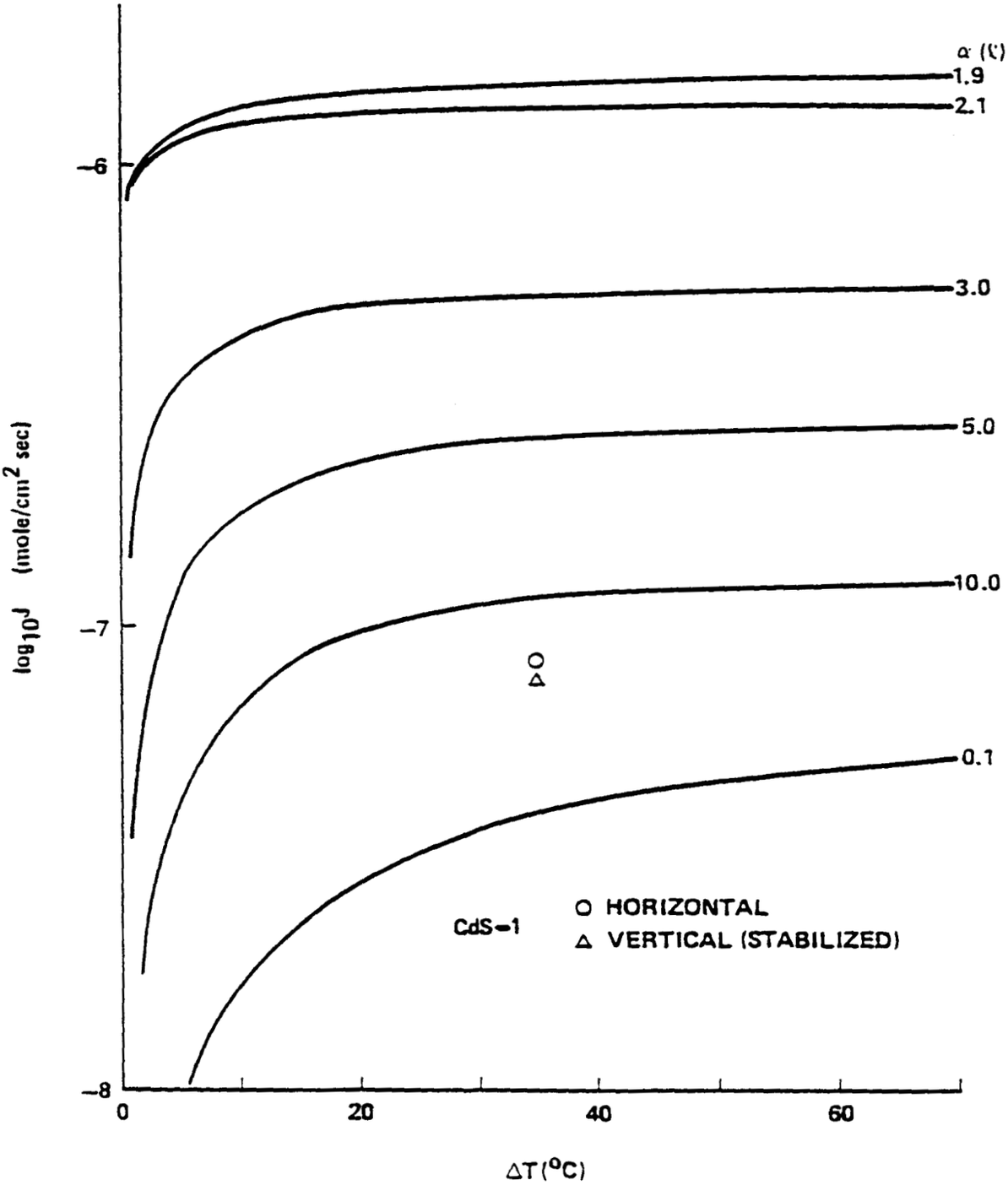
α (Ω)
1.9
2.1
3.0
5.0
10.0
0.1
−6
−7
−8
0
20
40
60
log10J (mole/cm2 sec)
ΔT(°C)
CdS-1
O HORIZONTAL
Δ VERTICAL (STABILIZED)

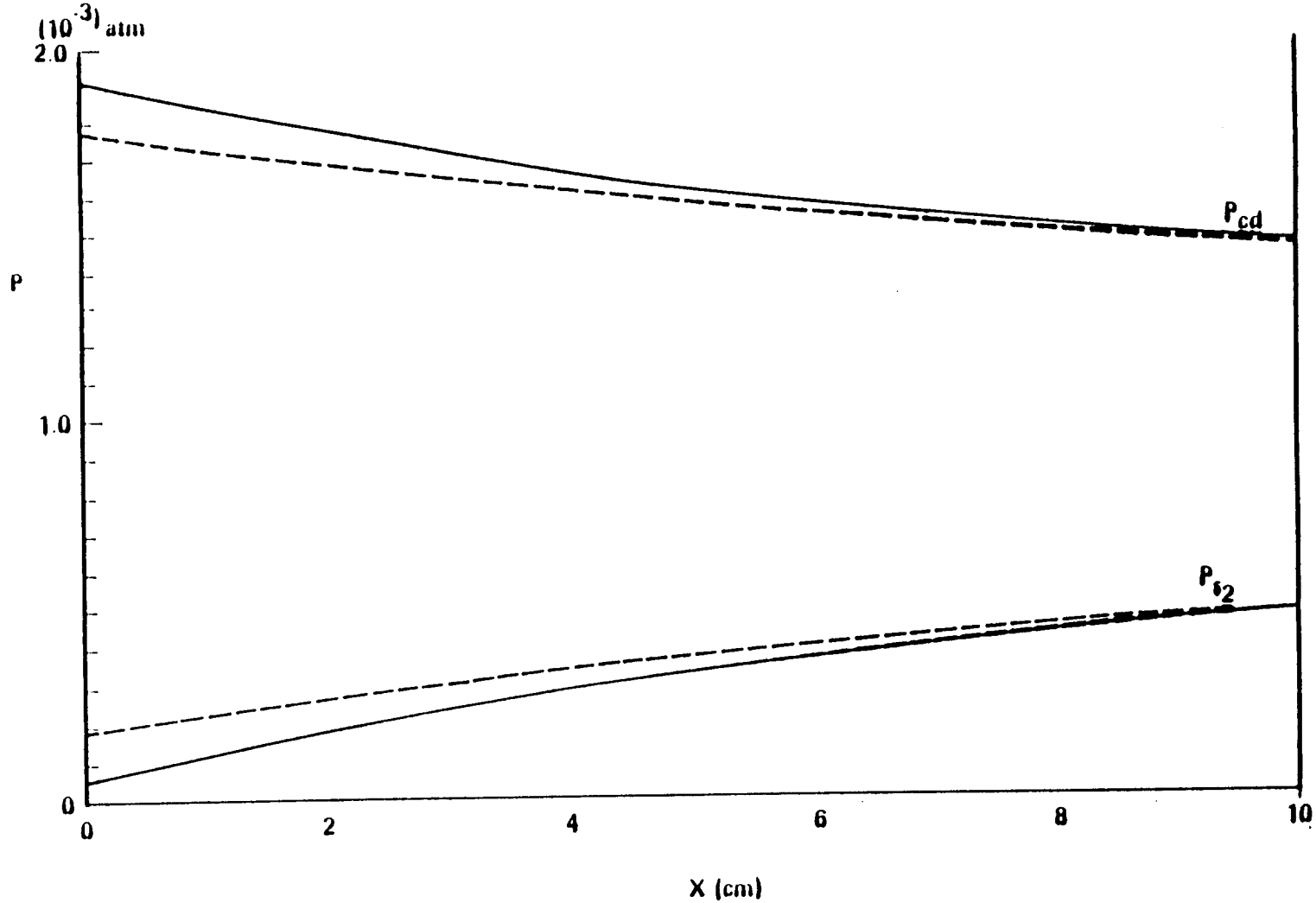
(10^{-3}) atm
2.0
1.0
0
P
P_{cd}
P_{O_2}
0
2
4
6
8
10
X (cm)

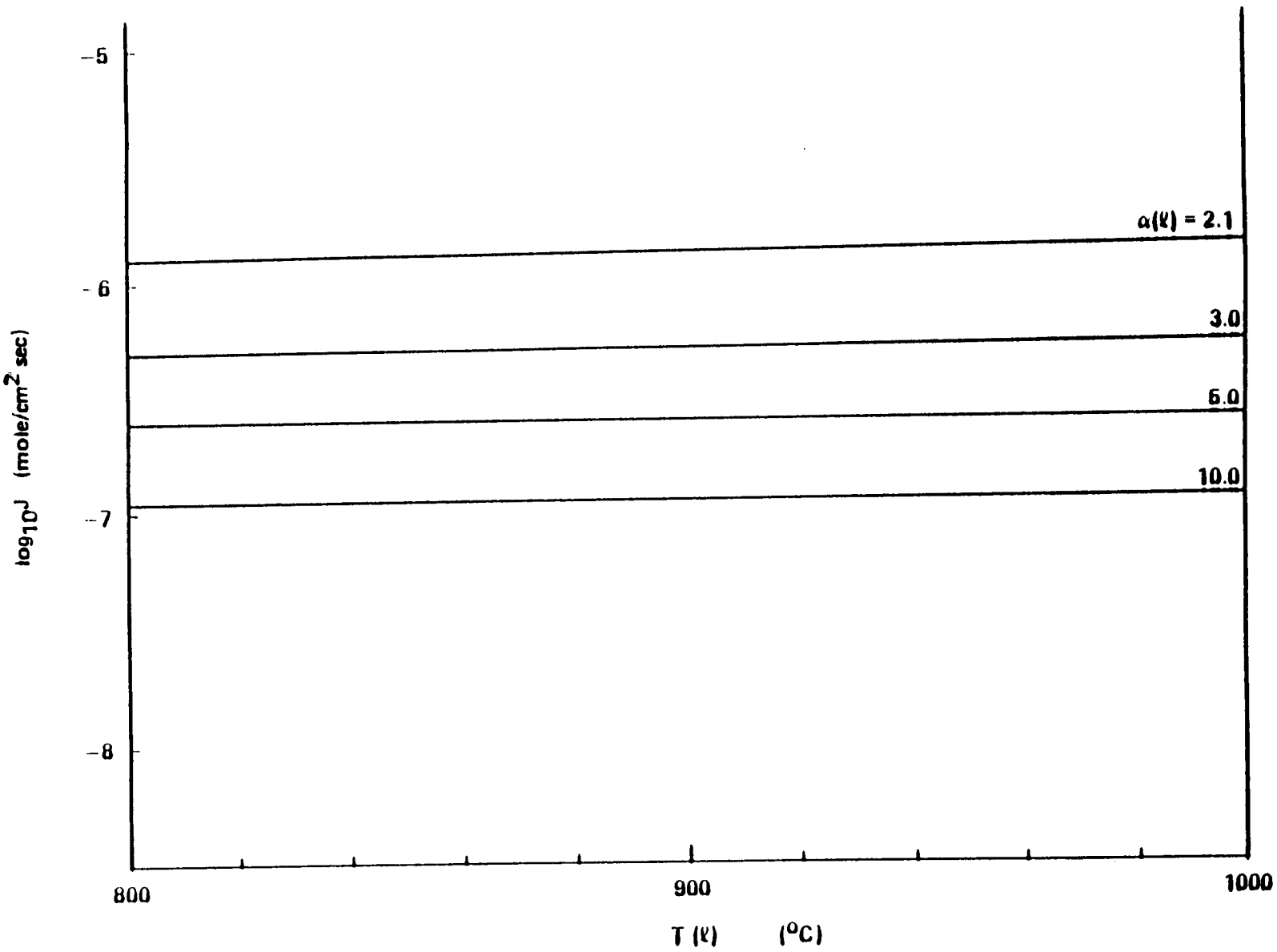
-5
-6
-7
-8
α(ℓ) = 2.1
3.0
5.0
10.0
log10J (mole/cm2 sec)
800
900
1000
T (ℓ) (°C)

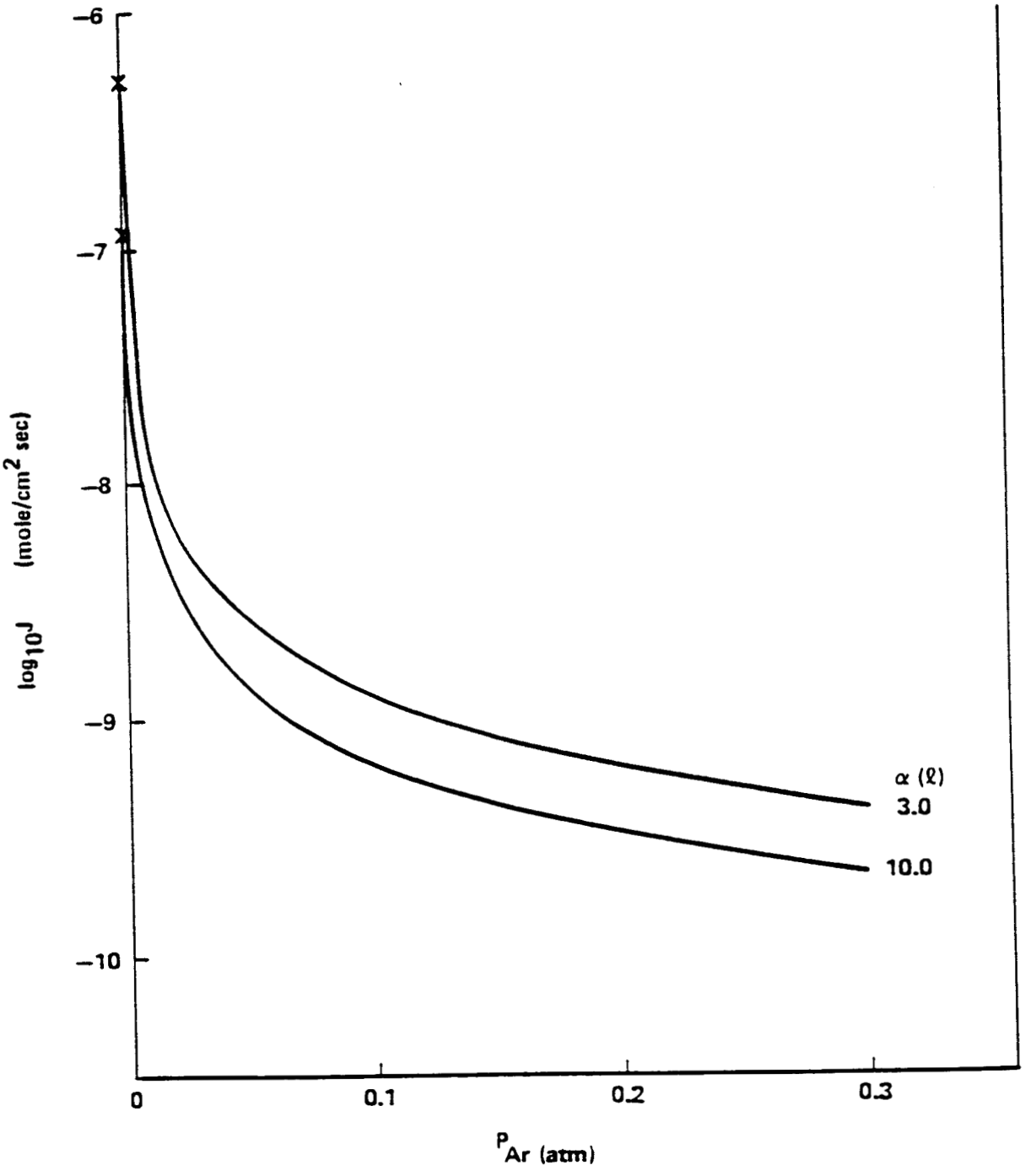
−6
−7
−8
−9
−10
$\log_{10} J$ (mole/cm^2 sec)
0
0.1
0.2
0.3
P_{Ar} (atm)
α (ℓ)
3.0
10.0

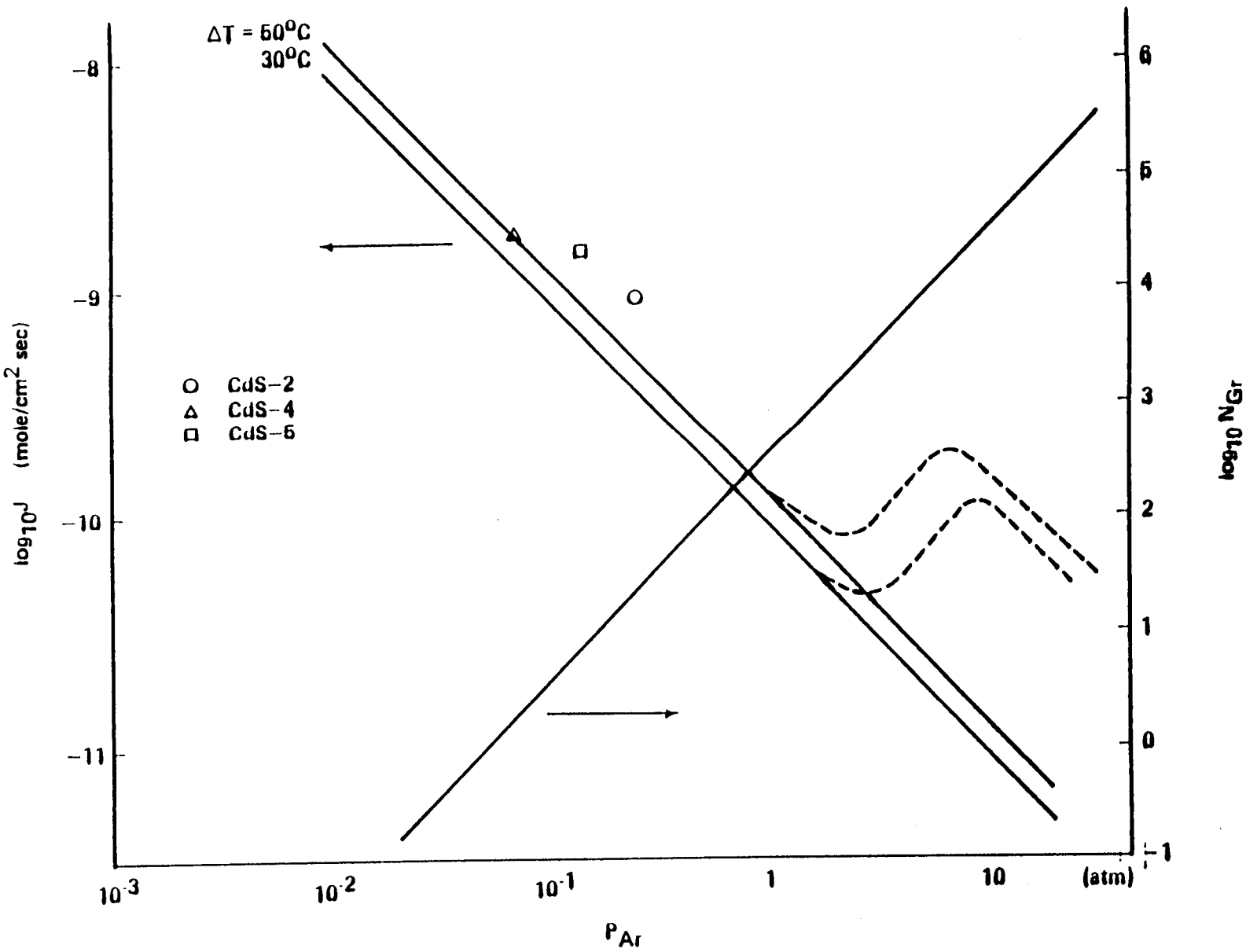
ΔT = 60°C
30°C
○ CdS-2
△ CdS-4
□ CdS-5
log10J (mole/cm2 sec)
log10 NGr
-8
-9
-10
-11
6
5
4
3
2
1
0
-1
10-3
10-2
10-1
1
10
(atm)
PAr

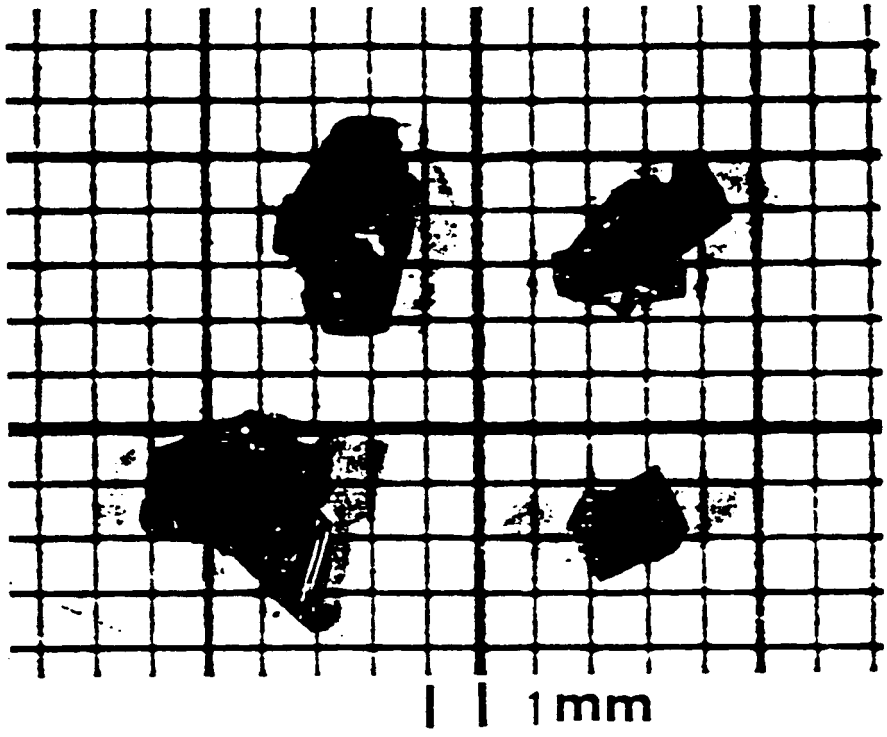
1mm

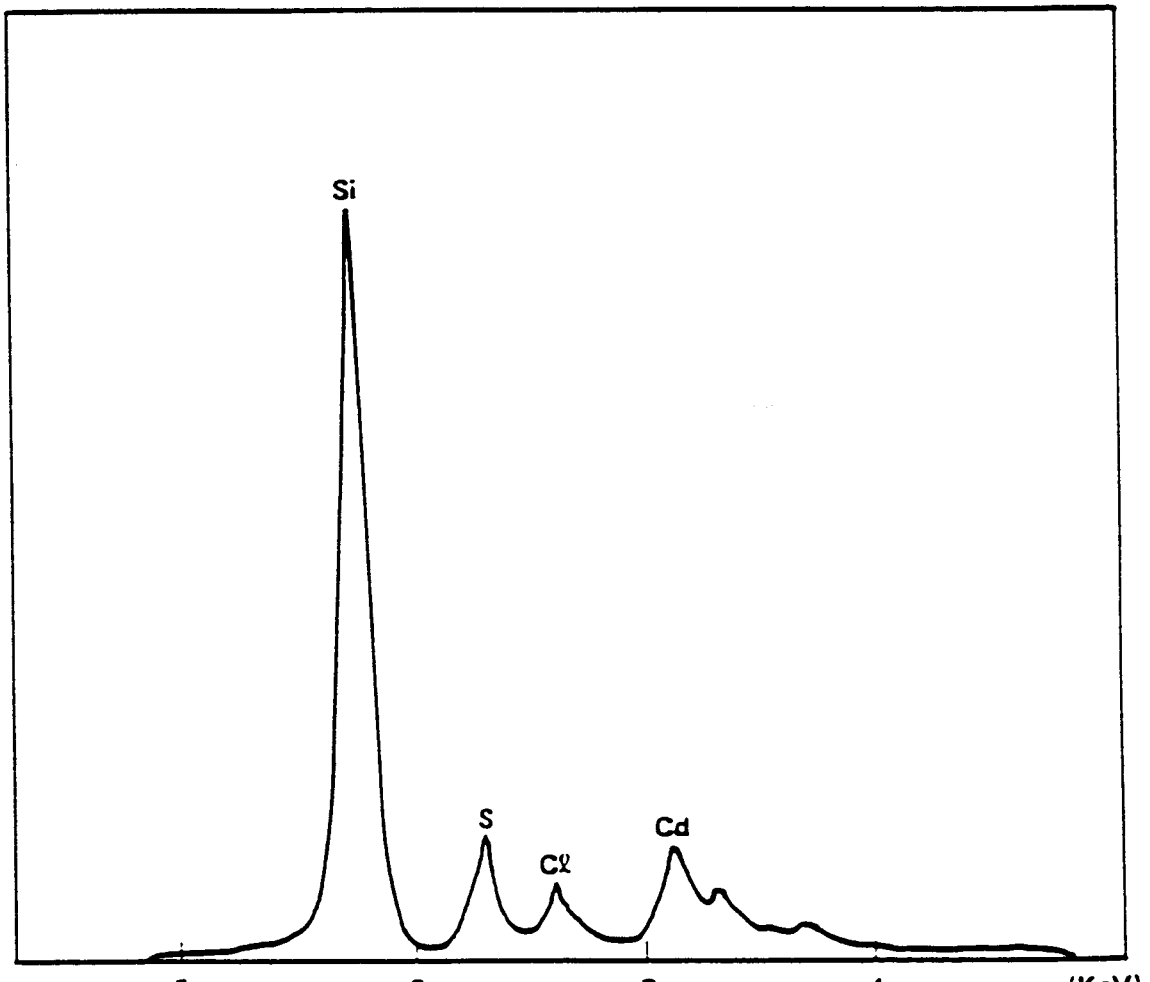

XES

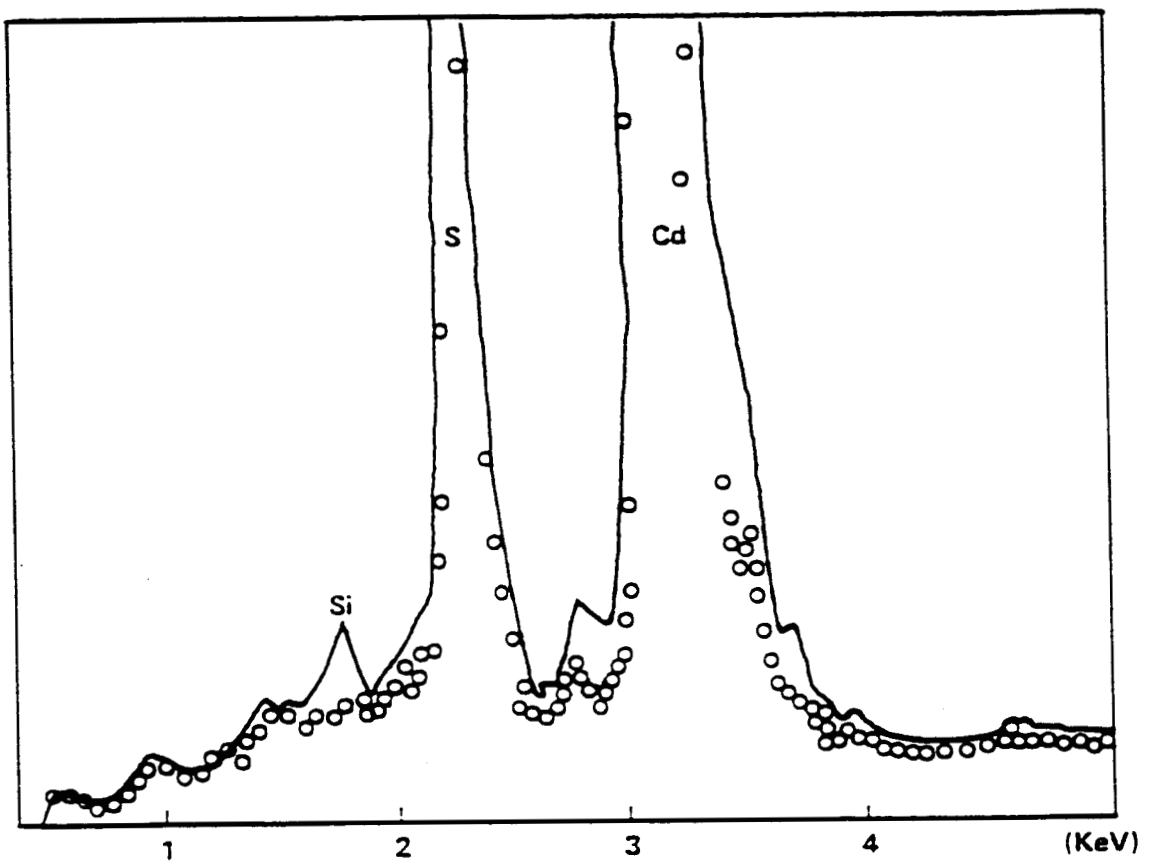

XES

POLYIMIDES CONTAINING OXYETHYLENE UNITS, III. ISOIMIDE PRECURSORS TO SEMICRYSTALLINE POLYIMIDES

Frank W. Harris, Andrea J. Karnavas,
Charles N. Cucuras and Sajal Das
Department of Polymer Science
The University of Akron
Akron, Ohio 44325

The overall objective of this ongoing research is the development of new thermally-stable composite resins for various aerospace applications. Although it is highly desirable that these polymers be soluble in order to facilitate processing, they must display considerable solvent-resistance in use. A recent approach has involved the synthesis of a new series of polyimides containing flexible linkages.[1,2] The polymers were prepared by the polymerization of aromatic dianhydrides with diamines containing oxyethylene linkages. For example, the polymerization of 3,3',4,4'-benzophenonetetracarboxylic dianhydride (BTDA, 1) with 2a-d afforded highly crystalline polyimides that were completely insoluble.[2] However, a polyimide that was amorphous and soluble was obtained from the polymerization of BTDA and an isomer of 2b, i.e., bis[2-(3-aminophenoxy)ethyl]ether (6).

The primary objective of this research was to investigate the synthesis of the isoimide isomers[3-5] of the insoluble polyimide systems. It was postulated that these materials would be soluble and would undergo thermally-induced isomerizations to the corresponding polyimides. Another objective of this work was to prepare block copolyimides from BTDA and diamines 2b and 6. It was hoped that a soluble, amorphous system would be obtained that could be annealed into an insoluble, semicrystalline state. If the block copolymers failed to display solubility, their isoimide isomers were to be prepared.

RESULTS AND DISCUSSION

Polyisoimide Precursors to Semicrystalline Polyimides

The polymerization of BTDA with 2 in NMP at ambient temperature gave the polyamic acids 3, which were treated with dicyclohexyl carbodiimide (DCC) to afford the corresponding polyisoimides (4) (Table 1). The bright-yellow polymers were soluble in NMP, DMF, DMSO and m-cresol. Upon heating to above 200°C, they isomerized to their imide form (5). Further heating to near 350°C resulted in the exothermic crystallization of the imide isomers. These polymers melted between 362° and 470°C.

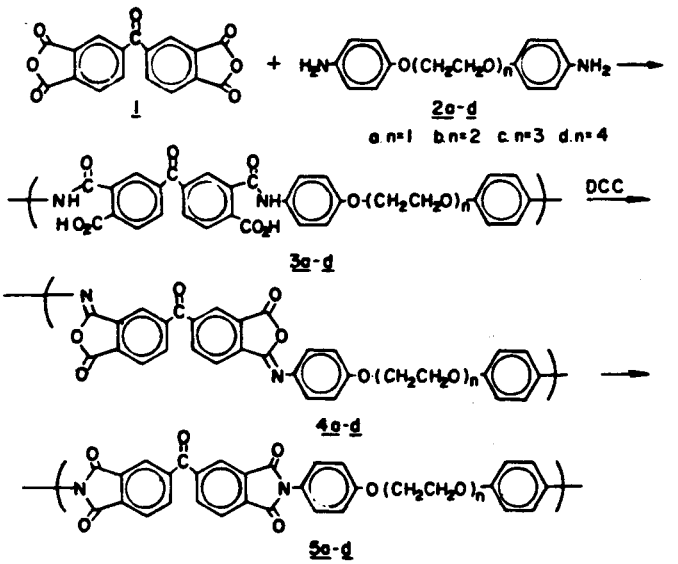

TABLE 1

Polyamic Acids, Polyisoimides and Polyimides From BTDA and Diamines 2a-d

Polyamic Acid		Polyisoimide			Polyimide			
Sample No.	$(\eta)^a$	Sample No.	$(\eta)^b$	$T^c_{I_{max}}$	Sample No.	$T^d_{C_{max}}$	T^e_m	TGA[f]
3a	0.89	4a	0.90	240	5a	-	470	485
3b	0.85	4b	0.64	245	5b	375	402	460
3c	0.91	4c	1.30	220	5c	365	405	432
3d	0.35	4d	0.33	238	5d	340	360	400

a. Inherent viscosity in NMP at 30°C with a concentration of 0.5 g/dl. Polyamic acid was not isolated prior to determination.

b. Inherent viscosity in NMP at 30°C with a concentration of 0.5 g/dl. Polyisoimide was isolated by precipitation in absolute ethanol prior to determination.

c. Temperature at which maximum in isomerization exotherm occurred on DSC thermogram obtained in N_2 with a heating rate of 20°C/min.

d. Temperature at which maximum in crystallization exotherm occurred on DSC thermogram obtained in N_2 with a heating rate of 20°C/min.

e. Temperature at which minimum in melting endotherm occurred on DSC thermogram obtained in N_2 with a heating rate of 20°C/min.

f. Temperature at which 5% weight loss occurred on TGA thermogram obtained in N_2 with a heating rate of 10°C/min.

Block Copolyimides

In an attempt to obtain a soluble, amorphous polyimide that could be annealed into a crystalline state, block copolymers of 2b and 6 and BTDA were prepared. Thus, BTDA was treated with excess 6 in NMP at ambient temperature to afford amine-terminated oligomers (7). Molar ratios of BTDA to 6 of 1:2 and 3:4 were used. These oligomers were then polymerized with various amounts of 2b and additional BTDA to afford a series of block copolyamic acids (8) (Table 2). The polyamic acids were imidized by thermal and chemical methods to afford the corresponding polyimides (9). Thermal imidization was apparently accompanied by some depolymerization as the viscosities of the polyimides were considerably less than their polyamic acid precursors.

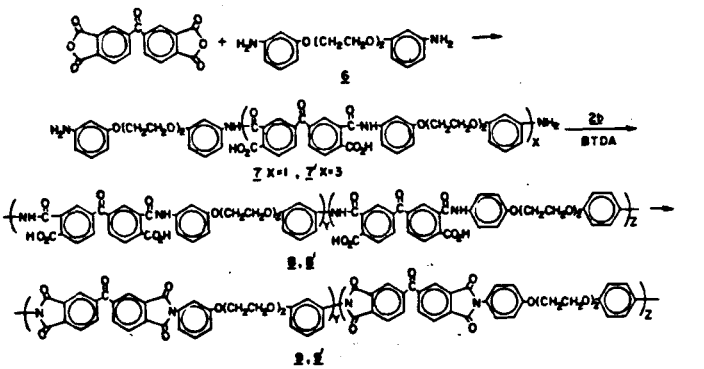

The copolymers containing less than 20 weight % 2b were soluble in organic solvents. However, these polymers did not display a T_m. Although copolymers containing higher levels of 2b displayed two T_g's and a T_m, they were insoluble (Table 3). As the level of 2b increased, the T_m increased and the intensity of the T_g near 215°C decreased. This is consistant with an increase in crystalline perfection in the 2b blocks.

TABLE 2

Block Copolyimides of Diamines 6 and 2b and BTDA

Molar Ratio of Oligomer to 2b	Thermal Imidization[a]			Chemical Imidization[b]		
	Polyamic Acid No.	Amic Acid $(\eta)^c$	Imide $(\eta)^d$	Polyamic Acid No.	Amic Acid $(\eta)^c$	Imide $(\eta)^d$
100:0	8aT	0.88	0.26	8aC	0.73	0.56
75:25[e]	8bT	0.81	0.27	8bC	0.65	-
50:50	8cT	0.84	-	8cC	0.80	-
25:75	8dT	0.67	-	8dC	0.70	-
100:0	8'aT	0.76	0.36	8'aC	0.33	0.21
75:25[f]	8'bT	0.73	0.29	8'bC	0.58	0.41
50:50	8'cT	0.75	-	8'cC	0.72	-
25:75	8'dT	0.71	-	8'dC	0.54	-

a. Solution of polyamic acid in NMP was heated to reflux, and the water of imidization was removed by distillation. Fresh NMP was continuously added to replace distillate. Distillation-addition cycle was carried out for 3 hr.
b. After the solution of polyamic acid in NMP was diluted to 6% solids with NMP, a 2 molar excess of an equimolar solution of pyridine and acetic anhydride was added. The resulting mixture was stirred overnight at ambient temperature.
c. Inherent viscosity of polyamic acid in NMP at 30°C with a concentration of 0.5 g/dl.
d. Inherent viscosity of polyimide i NMP at 30°C with a concentration of 0.5 g/dl.
e. 1:2 Molar ratio of BTDA to 6.
f. 3:4 Molar ratio of BTDA to 6.

TABLE 3

Thermal Properties of Block Copolyimides

Thermal Imidization			Chemical Imidization		
Sample No.	T_g	T_m	Sample No.	T_g	T_m
9aT	159	-	9aC	150	-
9bT	152	-	9bC	148	-
9cT	159,215	305	9cC	152,205	368
9dT	162,218	336	9dC	146	402
9'aT	150	-	9'aC	148	-
9'bT	148	-	9'bC	156	-
9'cT	152,215	-	9'cC	150,208	360
9'dT	160,215	315	9'dC	150	400

a. T_g and T_m were determined using DSC with a heating rate of 20°C/min in N_2.
b. TGA thermograms of all the samples showed 5% weight losses near 460°C in N_2 with a heating rate of 10°C/min.

Polyisoimide Precursors to Block Copolyimides

In order to obtain soluble precursors to the semicrystalline, block copolyimides, their isoimide isomers were prepared. Thus, an amine-terminated oligomer (10) was prepared from a 3:4 molar ratio of BTDA to 6 and then allowed to react with various amounts of 2b and BTDA. The resulting polyamic acids (11) were converted to the corresponding polyisoimides by treatment with DCC (12) (Table 4). The polymers, which were readily soluble in DMF, NMP, DMSO, and m-cresol, underwent isomerization above 200°C to their imide form.

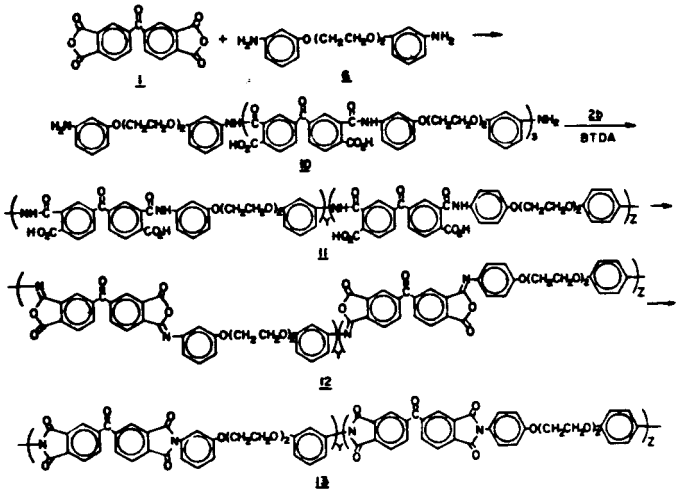

TABLE 4

Block Copolyamic Acids, Copolyisoimides, and Copolyimides

Molar Ratio of Oligomer[a] to 2b	Polyamic Acid		Polyisoimide			Polyimide	
	Sample No.	$(\eta)^b$	Sample No.	$(\eta)^c$	$T_{I_{max}}$[d]	Sample No.	T_m[e]
100:0	11a	0.82	12a	0.83	250	13a	
75:25	11b	0.68	12b	0.58	255	13b	343
50:50	11c	0.88	12c	0.92	250	13c	345
25:75	11d	0.85	12d	-	255	13d	372
0:100	11e	0.85	12e	0.64	245	13e	400

a. Oligomer was prepared from a 3:4 molar ratio of BTDA to 6.
b. Inherent viscosity in NMP at 30°C with a concentration of 0.5 g/dl. Polyamic acid was not isolated prior to determination.
c. Inherent viscosity in NMP at 30°C with a concentration of 0.5 g/dl. Polyisoimide was isolated by precipitation in absolute ethanol prior to determination.
d. Temperature at which maximum in crystallization exotherm occurred on DSC thermogram obtained in N_2 with a heating rate of 20°C/min.
e. Temperature at which minimum in melting endotherm occurred on DSC thermogram obtained in N_2 with a heating rate of 20°C/min.

ACKNOWLEDGMENT

The support of this research by the NASA-Langley Research Center under Grant No. NAG-1-448 is gratefully acknowledged. Appreciation is also expressed to Paul M. Hergenrother, NASA-Langley Materials Division, for his helpful suggestions.

LITERATURE CITED

1. W.A. Feld, B. Ramalingam and F.W. Harris, J. Polym. Sci., Polym. Chem. Ed., 21, 319 (1983).
2. F.W. Harris, M.W. Beltz and S. Das, Polym. Preprints, 25(1), 160 (1984).
3. R. J. Angelo, U.S. Patent 3,282,898 (1966).
4. R.A. Dine-Hart and W.W. Wright, J. Appl. Polym. Sci., 11, 609 (1967).
5. A.L. Landis and A.B. Naselow in "Polyimides: Synthesis, Characterization, and Applications," Vol. 1, K. L. Mittal, Ed., Plenum, NY, 1984, pp. 39-49.